

## ON THE NUMERICAL MODELING OF IMPINGING JET HEAT TRANSFER

Mirko Bovo<sup>1,2</sup>, Sassan Etemad<sup>2</sup> and Lars Davidson<sup>1</sup>

<sup>1</sup> Dept. of Applied Mechanics, Chalmers University of Technology, Gothenburg, Sweden

<sup>2</sup> Powertrain Analysis, Volvo Car Corporation, Gothenburg, Sweden

**ABSTRACT.** Steady state numerical simulation of impinging jet heat transfer at  $H/D = 2$  is methodically investigated for the following parameters: Turbulence models ( $k-\epsilon$  low Re,  $k-\omega$  low Re and V2F), grid density (0.25E06, 0.5E06, 1E06 and 2E06 cells), grid topology (2 types), inlet velocity corresponding to Re (10000, 20000 and 30000) and inlet velocity profile (uniform flow and fully developed flow). Effect of numerical discretization scheme is also investigated. The study resulted in 95 simulations. The simulation results are compared with different published experimental data. It was found that the V2F turbulence model performs best for these types of simulations. Furthermore, the choice of turbulence model and inlet velocity profile significantly affects the results. Grid topology is also found to be important. Careful CFD simulations are capable of predicting the heat transfer of impinging jets with good accuracy. (This work can be seen as a best practice guide for this type of simulations).

### INTRODUCTION

When fuel is sprayed in the combustion chamber of a reciprocating internal combustion engine, the resulting flow impinging on the cylinder wall presents jet like features. In this case many physical phenomena occur simultaneously. The spray brakes up, evaporates, ignites, burns and eventually meets the cylinder wall as a jet like-flame. Moreover, the whole process is transient (cyclic). Due to its inherent characteristics, the spray combustion process is difficult to measure and to model numerically. Meanwhile, due to the desire for more efficient engines, there is a growing need for a better understanding of the physics in the engine combustion chamber.

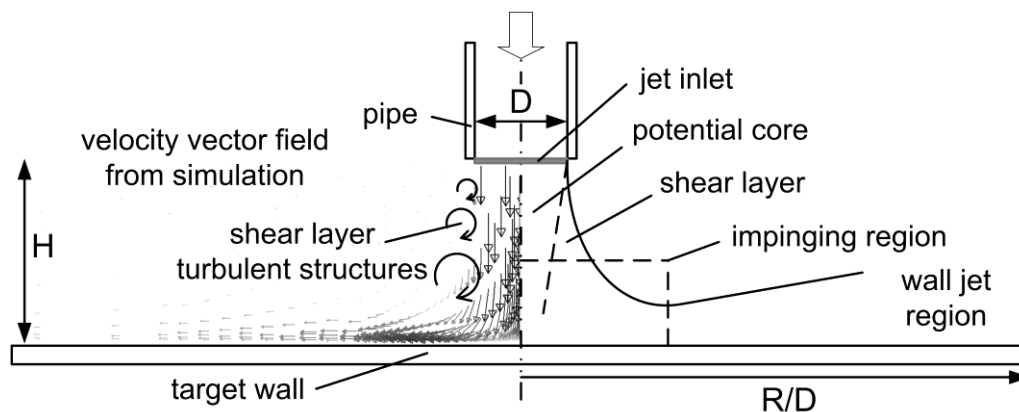


Figure 1. Impinging jet qualitative region definition (right). Impinging jet flow field (left)

Beside internal combustion engines, cases involving heat transfer due to impinging jets are common in industry. This type of flow has among the highest levels of Nusselt number (Nu) known for single

phase flows. Impinging jets are used where high rates of heat transfer are needed, for example in the cooling of electronic devices or turbine blades.

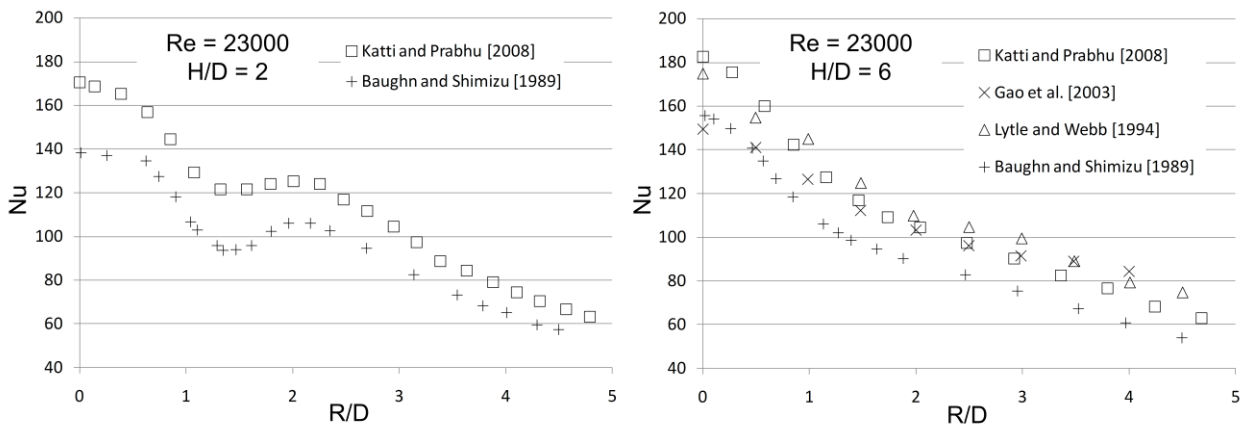


Figure 2. Published experimental results of  $Nu(R/D)$ . In the left figure, data from Baughn and Shimizu [1989] at  $H/D = 2$  and  $Re = 23750$  are scaled to  $Re = 23000$  using correlations proposed by Katti and Prabhu [2008]

Impinging jet heat transfer depends on several parameters, for example jet  $Re$ , nozzle shape, nozzle diameter ( $D$ ) and nozzle-wall distance ( $H$ ). For relatively high  $Re$  and small  $H/D$  (e.g.  $Re = 23000$  and  $H/D = 2$ ) the local Nusselt number variation in radial direction  $Nu(R/D)$  presents a secondary peak as shown in Figure 2 (left). This phenomenon is not fully understood despite considerable experimental, analytical and numerical efforts [e.g. Gao, et al. 2003, 2006, O'Donovan and Murray 2007]. Various possible explanations are suggested to explain the characteristic secondary peak:

- The flow accelerates in radial direction exiting the impingement zone. High velocity is associated with high heat transfer.
- The boundary layer develops from the stagnation point becoming turbulent and locally increasing the heat transfer rate.
- Turbulent structures grow in the shear layer of the jet (see Figure 1). These structures travel in the jet direction and impact on the target surface in a ring around the impingement point. Resulting velocity fluctuations normal to the wall increase the heat transfer.

Most likely, the interaction of all the presented reasons is the cause of the observed phenomena.

Flow measurements are not trivial. Several authors have published experimental results using different optical measuring techniques. Figure 2 (right) shows measurements of  $Nu(R/D)$  from four different authors. Statistical analysis of the data shows an average spreading of about 10% from the mean value.

In CFD, new turbulence models are applied to generic, well documented cases to evaluate their performance. Often the models are tested in simplified conditions, for example 2D cases with symmetric boundary conditions. However, there is a risk that well performing models in such conditions will fail to work for real industrial applications, due to stability problems and poor robustness. Furthermore, even if a model fails to accurately predict absolute values, it might, however, be able to predict trends correctly, which is certainly of great industrial interest. Therefore, robust models such as the  $k-\epsilon$  are still widely used in industry.

Impinging jets are notoriously difficult to model in CFD. The flow features of the near wall region are difficult to capture with the common near wall assumptions implemented in the models. Moreover, the flow field presents strong curvatures, unsteadiness and strong pressure strain stresses. The combination of these features makes it difficult to accurately predict the impinging jet flow and consequently its associated convective heat transfer.

This work has the purpose of evaluating the state of the art of the steady state CFD models with complete circular grid for an impinging jet at  $H/D = 2$ . The influences of several variables are systematically studied using the factorial design of experiment approach. The variables investigated are: Turbulence models (low Re  $k-\epsilon$ , low Re  $k-\omega$ , V2F), grid density ( $0.25E06$ ,  $0.5E06$ ,  $1E06$  cells), grid topology (2 types) and  $Re_D$  (10000, 20000, 30000). The calculated Nusselt number is compared with available experimental data. In addition, further simulations are carried out for a selected subset of parameters to investigate the effect of inlet velocity profile (uniform flow and fully developed) and grid density ( $0.25E06$ ,  $0.5E06$ ,  $1E06$  and  $2E06$  cells). The study includes a total of 95 simulations.

### MODELING METHODOLOGY

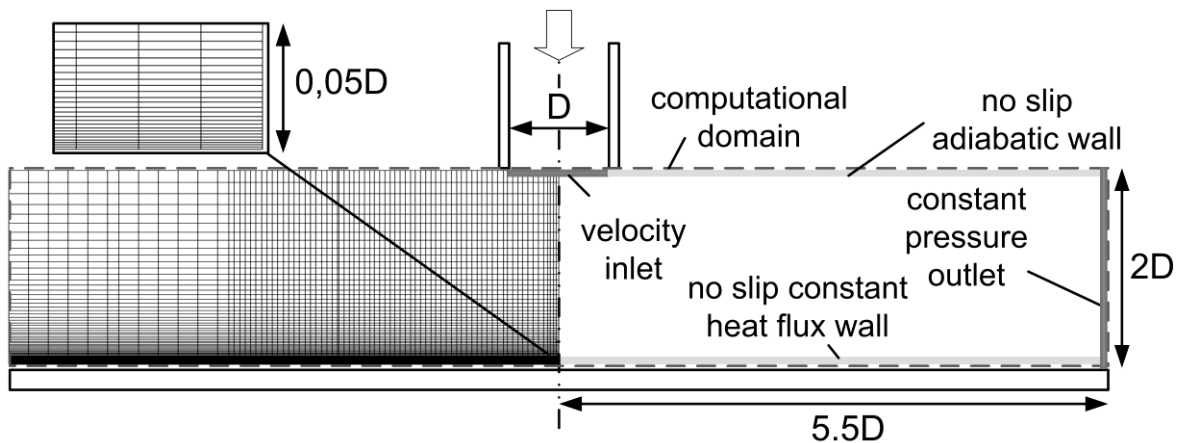


Figure 3. Computational domain and spatial discretization grid in axial direction

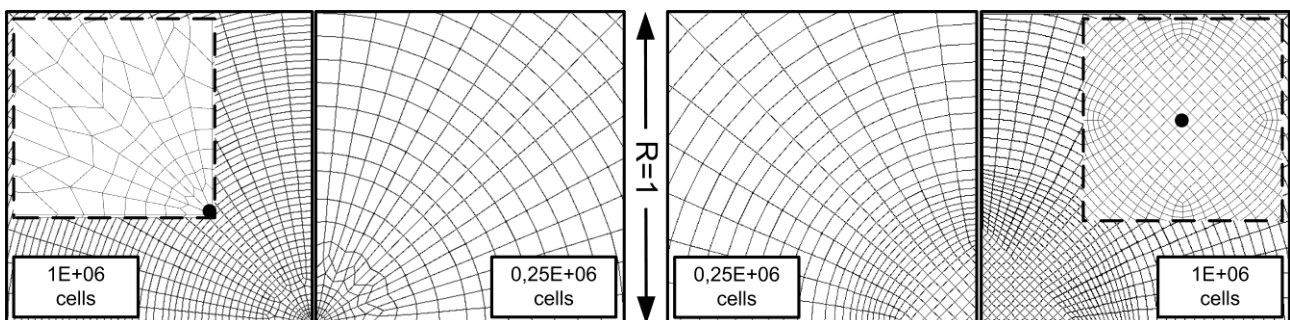


Figure 4. Peacock (left) and Butterfly (right) grid topology. Note that butterfly topology allows only for radial cell density growth while the peacock includes also angular growth. The black dot in the zoomed images represents the grid center.

**Computational domain** The computational domain is shown in Figure 3. All geometrical dimensions are normalized with the inlet diameter  $D$ . The computational domain extends to a radius of

5.5D and a height of 2D. (The pipe is not included in the simulations). The computational domain is a complete circular region.

**Grid** The grid cross-section in axial direction is shown in Figure 3. The near wall cell thickness adjacent to the wall satisfies  $y^+ < 1$  in the entire domain for all cases. The number of cells in the direction normal to the wall is kept constant for the grid independency study. The features of the two different grid topologies are defined in Figure 4. Both topologies result in fully hexahedral structured grids. The topology called “butterfly” is based on a square outline in the center that is transformed in a circular shape. This topology allows only for refinement in radial direction for a given partition of the inner square. The topology called “peacock” can be adapted to discretize any angle. In addition, it allows for grid refinement in both radial and angular directions.

**Boundary conditions** In general, boundary conditions are selected to be as close as possible to the experimental conditions. This is not always easy to implement and simplifications need to be made. The boundary conditions used are presented and discussed one by one.

Inlet boundary The Inlet Boundary condition is one of the investigated parameters. The impact of uniform flow (plug flow) and fully developed pipe flow are compared. The inlet profile corresponding to fully developed pipe flow is generated with a separate simulation using the V2F model. An infinitely long pipe is simulated by application of cyclic boundary conditions to a short pipe. The variables resulting from the cyclic simulation are mapped as inlet boundary condition for the impinging jet simulations. The mapped variables are: velocity, turbulent kinetic energy and its dissipation rate.

Outlet Constant pressure is used as outlet boundary condition.

Target wall The target wall is defined as no-slip wall with constant wall heat flux.

Upper boundary The upper non-wall fluid boundary is set to adiabatic no-slip wall and consequently defines a confined jet. However, this is not believed to sensibly affect the results. The differences in heat transfer between confined and unconfined jet for  $H/D \geq 2$  are shown to be negligible by Gao and Ewing [2006].

**Turbulence model** The turbulence models used are: standard low Reynolds number  $k$ - $\epsilon$ , standard low Reynolds number  $k$ - $\omega$  and V2F. These models are hereafter referred to as  $k$ - $\epsilon$ ,  $k$ - $\omega$ , and V2F. Both  $k$ - $\epsilon$  and  $k$ - $\omega$  are, so called, two-equation model. They model the turbulence by solving the transport equation for two turbulent quantities, namely  $k$  and  $\epsilon$  or  $\omega$ . The low Re implementations implies that the boundary layer is resolved to the wall including the viscous sub-layer. This allows for an accurate solution of the flow field close to the wall at the expense of a higher computational cost. The V2F differs from the common two-equations models in that in addition to  $k$  and  $\epsilon$  it solves for two additional quantities, the wall-normal Reynolds stress  $v^2$  and its redistribution function  $f_{22}$ . The V2F model requires a fine near wall grid.

The transport equations for the different turbulence models are given below in their steady state incompressible form. The equation for the turbulent kinetic energy,  $k$ , is the same for all models as is as follows

$$\frac{\partial}{\partial x_j} \left[ \rho u_j k - \left( \mu + \frac{\mu_t}{\sigma_k} \right) \frac{\partial k}{\partial x_j} \right] = \mu_t \left( 2S_{ij} \frac{\partial u_i}{\partial x_j} \right) - \rho \epsilon \quad (1)$$

With

$$S_{ij} = \frac{1}{2} \left( \frac{\partial u_i}{\partial x_j} + \frac{\partial u_j}{\partial x_i} \right) \quad (2)$$

$$\mu_t = f_\mu \frac{C_\mu \rho k^2}{\varepsilon} \quad (3)$$

Where the damping function  $f_\mu$  is defined for each model and  $\varepsilon = \beta^* k \omega$  in the k- $\omega$  model. The equations for the turbulent dissipation rate  $\varepsilon$  for the k- $\varepsilon$  model is the following

$$\begin{aligned} \frac{\partial}{\partial x_j} \left[ \rho u_j \varepsilon - \left( \mu + \frac{\mu_t}{\sigma_\varepsilon} \right) \frac{\partial \varepsilon}{\partial x_j} \right] \\ = C_{\varepsilon 1} \frac{\varepsilon}{k} \left[ \mu_t \left( 2S_{ij} \frac{\partial u_i}{\partial x_j} + P' \right) \right] + C_{\varepsilon 2} (1 - 0.3e^{-R_t^2}) \rho \frac{\varepsilon^2}{k} + C_{\varepsilon 4} \rho \varepsilon \frac{\partial u_i}{\partial x_i} \end{aligned} \quad (4)$$

With

$$P' = 1.33 [1 - 0.3e^{-R_t^2}] \left[ 2S_{ij} \frac{\partial u_i}{\partial x_j} + 2 \frac{\mu}{\mu_t} \frac{k}{y^2} \right] e^{-0.00375 Re_y^2} \quad (5)$$

$$f_\mu = [1 - e^{-0.0198 Re_y}] \left( 1 + \frac{5.29}{Re_y} \right) \quad (6)$$

$$Re_y = \frac{y \sqrt{k}}{\nu} \quad (7)$$

$$R_t = \frac{k^2}{\nu \varepsilon} \quad (8)$$

Table 1  
 Coefficients for the k- $\varepsilon$  turbulence model

$C_\mu$	$\sigma_k$	$\sigma_\varepsilon$	$C_{\varepsilon 1}$	$C_{\varepsilon 2}$	$C_{\varepsilon 4}$
0.09	0.75	1.15	1.15	1.9	-0.33

A complete description of the k- $\varepsilon$  model can be found in Lien, et al. [1996]. A similar implementation is developed for the specific turbulence dissipation rate,  $\omega$ , in the k- $\omega$  model and can be found in Wilcox [1998]. The transport equation for  $\varepsilon$  in the V2F model is

$$\frac{\partial}{\partial x_j} \left[ \rho u_j \varepsilon - \left( \mu + \frac{\mu_t}{\sigma_\varepsilon} \right) \frac{\partial \varepsilon}{\partial x_j} \right] = \frac{C_{\varepsilon 1}^Z}{T_s} \left[ \mu_t \left( 2S_{ij} \frac{\partial u_i}{\partial x_j} \right) \right] - \frac{C_{\varepsilon 2}}{T_s} \rho \varepsilon \quad (9)$$

The  $v^2$  equation is

$$\frac{\partial}{\partial x_j} \left[ \rho u_j \overline{v^2} - \left( \mu + \frac{\mu_t}{\sigma_k} \right) \frac{\partial \overline{v^2}}{\partial x_j} \right] = \rho k f_{22} - 6 \rho \overline{v^2} \frac{\varepsilon}{k} \quad (10)$$

The  $f_{22}$  equation is

$$L^2 \nabla^2 f_{22} - f_{22} = \frac{1 - C_1}{T_s} \left( \frac{2}{3} - \frac{\overline{v^2}}{k} \right) - C_2 \frac{\mu_t 2 S_{ij} \frac{\partial u_i}{\partial x_j}}{\rho k} - 5 \frac{\overline{v^2}/k}{T_s} \quad (11)$$

With

$$L = C_L \sqrt{\max \left( \frac{k^3}{\varepsilon^2}, C_\eta^2 \left( \frac{v^3}{\varepsilon} \right)^{1/2} \right)} \quad (12)$$

$$T_s = \max \left[ \frac{k}{\varepsilon}, C_{kT} \left( \frac{v}{\varepsilon} \right)^{1/2} \right] \quad (13)$$

$$\mu_t = \rho C_\mu \overline{v^2} T_s \quad (14)$$

$$C_{\varepsilon_1}^z = 1 + 0.045 \sqrt{k/\overline{v^2}} \quad (15)$$

Table 2  
 Coefficients for the V2F turbulence model

$C_\mu$	$\sigma_k$	$\sigma_\varepsilon$	$C_{\varepsilon 1}$	$C_{\varepsilon 2}$	$C_1$	$C_2$	$C_L$	$C_\eta$	$C_{kT}$
0.22	1.0	1.3	1.4	1.9	1.4	0.3	0.23	70.0	6.0

Notably, no damping function is used in the V2F model. A complete description of the V2F model and the values for the coefficients can be found in Durbin [1995].

**Medium** Air is used as fluid, it is simulated as incompressible since the  $Ma \ll 0.3$  in the entire domain.

**Solver** Equations for conservation of mass, momentum, energy and turbulent quantities are solved using the Navier-Stokes solver Star-CD V4.

**Convergence strategy** Every simulation is initialized with a zero velocity field and run with first (1<sup>st</sup>) order upwind discretization scheme. The simulations are allowed to run for a maximum of 4000 iterations. The convergence criterion is set to 1E-03 for all monitored residuals. 1<sup>st</sup> order converged simulations are restarted with the second (2<sup>nd</sup>) order discretization scheme “MARS” with 0.5 blending factor for the momentum, pressure and temperature equations. These simulations are run for a maximum of 4000 iterations. This strategy is used to help convergence and allows for comparison between results obtained with 1<sup>st</sup> and 2<sup>nd</sup> order discretization schemes. The maximum run time for a simulation with such convergence strategy is about 12h on 4 parallel compute nodes equipped with dual Intel Xeon X5460 (Quad-core, 3.16GHz).

## RESULTS AND DISCUSSION

The simulations generate a large amount of results to evaluate. These are mainly summarized in diagrams, pictures and graphs. The results are discussed below addressing the different parameters investigated. The first group of 54 simulations is run to allow cross evaluation of 5 different parameters (turbulence model, grid density, grid topology, numerical discretization, Re). Depending on the results a second, less extensive group of simulations is run to further investigate the grid density and the inlet velocity profile effects.

**Turbulence model** Figure 5 illustrates how the choice of turbulence model impacts the results. It was found that the turbulence model is the most influencing parameter.

*k-ε* From Figure 5 it is visible that *k-ε* consistently over-predicts the heat transfer in the stagnation zone. It performs often well for  $R/D > 2$  but its performance is inconsistent in this region where it occasionally under-predicts the experimental results significantly. No particular cause is found to explain this deviation.

*k-ω* Figure 6 shows that *k-ω* is the most successful model in converging with a 2<sup>nd</sup> order discretization scheme. *k-ω* gives consistently good agreement with experiments for small  $R/D$  ( $< 1.5$ ) but deviates for greater  $R/D$  (see Figure 5). The spreading effect for  $R/D > 4$  is possibly due to the outlet boundary and is common for all models.

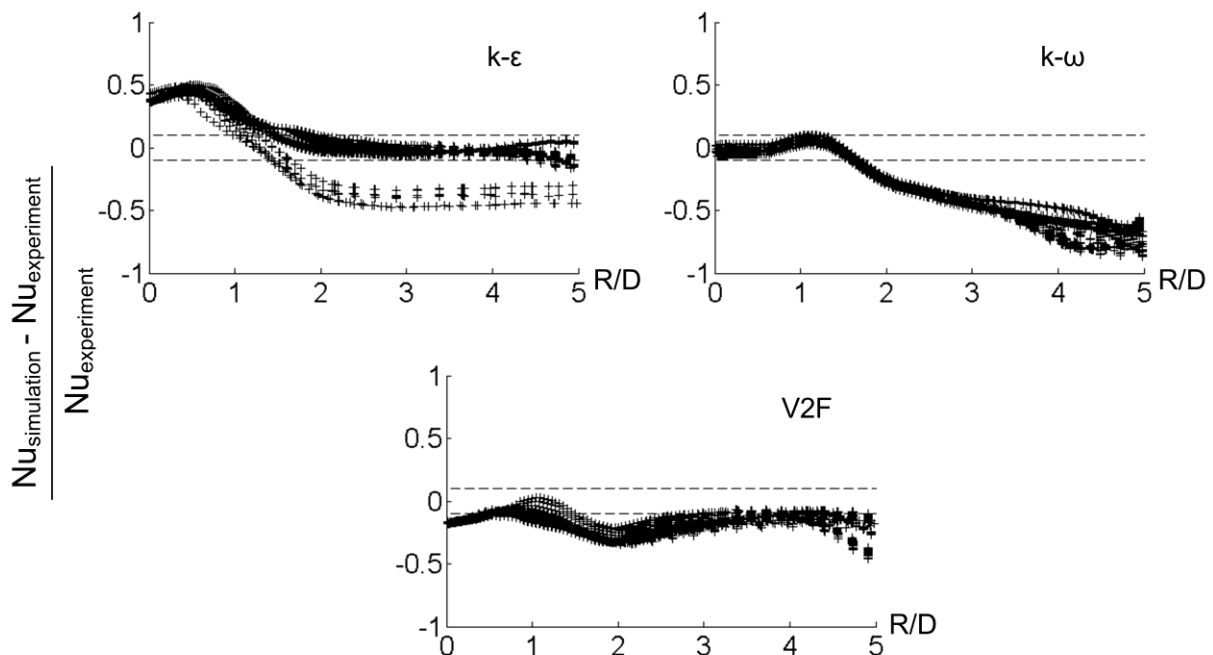


Figure 5. Simulation results for  $Re = 20000$  compared with linear interpolation of experimental results from Baughn and Shimizu [1989] and Katti and Prabhu [2008]. Available data from Baughn and Shimizu [1989] are scaled as in Figure 2. All converged simulations are displayed (9 for *k-ε*, 12 for *k-ω*, 7 for V2F). For each simulation all wall cell values are displayed. The  $\pm 0.1$  stripe represents 10% deviation from the average of the two experimental sets

**V2F** V2F seems to be insensitive to all other parameters (discretization scheme, grid density and topology) as can be seen in Figure 5. It displays a more constant offset from the experimental data for all R/D, somehow under-estimating the experimental results. The spreading in the range  $1 < R/D < 2$  occurs for simulations with fine grid and 2<sup>nd</sup> order discretization scheme. This spreading derives from the fact that the solution is not fully axisymmetric. It is believed that transient phenomena are the cause of this effect. Figure 6 shows that the V2F model reaches convergence with 2<sup>nd</sup> order discretization scheme only for a few cases, however, the net average difference in Nu between solution obtained with 1<sup>st</sup> and 2<sup>nd</sup> order discretization scheme for this model is below 3.3%. This gives confidence on the successfulness of V2F. In other words, better a solution obtained with the V2F model and 1<sup>st</sup> order discretization scheme converged than one obtained using the k- $\omega$  model with a 2<sup>nd</sup> order discretization scheme.

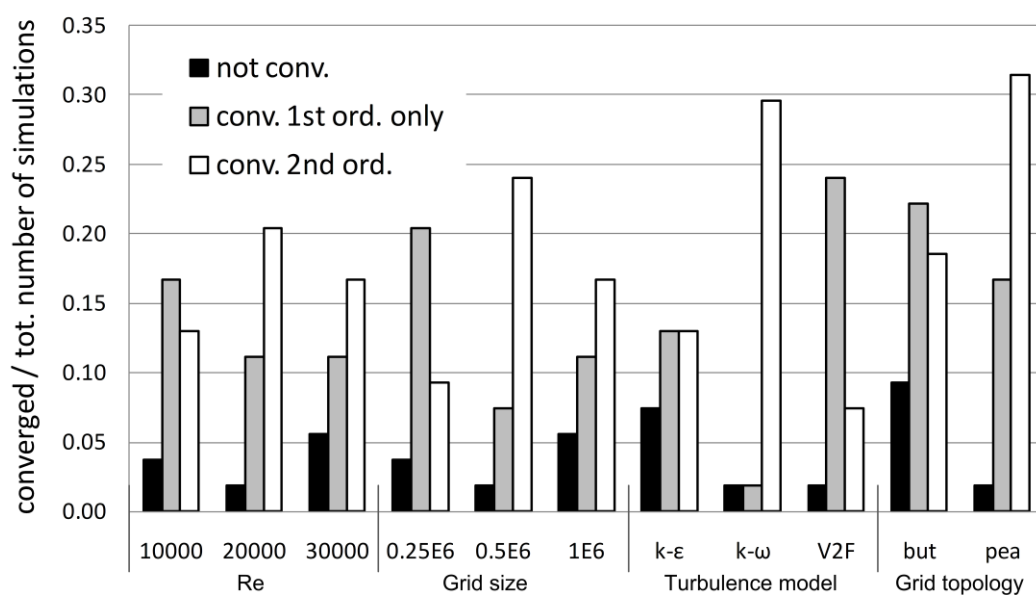


Figure 6. Convergence success relative to parameter. From left Re, grid size, turbulence model and grid topology (but = butterfly and pea = peacock)

**Grid size** A peak in convergence successfulness is reported for a grid size of 0.5E+06 cells (see Figure 6). A possible explanation is coarser grids are unable to resolve the flow features correctly. Finer grids, on the other hand, fail to converge to a steady solution because of the existing transient phenomena. Moreover, finer grids generally need more iterations to converge. However, for consistency, all simulations were limited to 4000 iterations in this study.

**Numerical discretization scheme** Out of 54 simulations, 47 (87%) converged using the 1<sup>st</sup> order numerical discretization scheme, among these, 27 (50%) converged also using the 2<sup>nd</sup> order scheme. In Figure 6 is shown the convergence relative to the parameters (Re, grid density, turbulence model, and grid topology). In general, the residuals plot for the non-converged simulations showed a stable cyclic fluctuation. This effect is characteristic of CFD simulations dominated by transient phenomena.

The net average difference in Nusselt number between 1<sup>st</sup> and 2<sup>nd</sup> order discretization scheme is 3.8% for the k- $\epsilon$  model, 3% for the k- $\omega$  model and 3.3% for the V2F model. Solutions using a 2<sup>nd</sup> order scheme are more accurate than 1<sup>st</sup> order ones and are recommended. However, 1<sup>st</sup> order discretization

scheme can still be considered physically representative and be used if 2<sup>nd</sup> order discretization scheme are difficult to obtain. This is recommended if the user has already found confidence in the model.

**Grid topology** Figure 6 shows that the grid topology called “peacock” is sensibly more successful than the one called “butterfly” in reaching a converged solution with a 2<sup>nd</sup> order discretization scheme. Further analysis indicates that, in average, peacock grids give closer results to the experimental data. Peacock topology offers more flexibility than butterfly topology. Indeed it allows for spatial refinement in both radial and angular directions. Moreover, peacock grid strategy can be used to discretize partial-circles of arbitrary angles (see Figure 4).

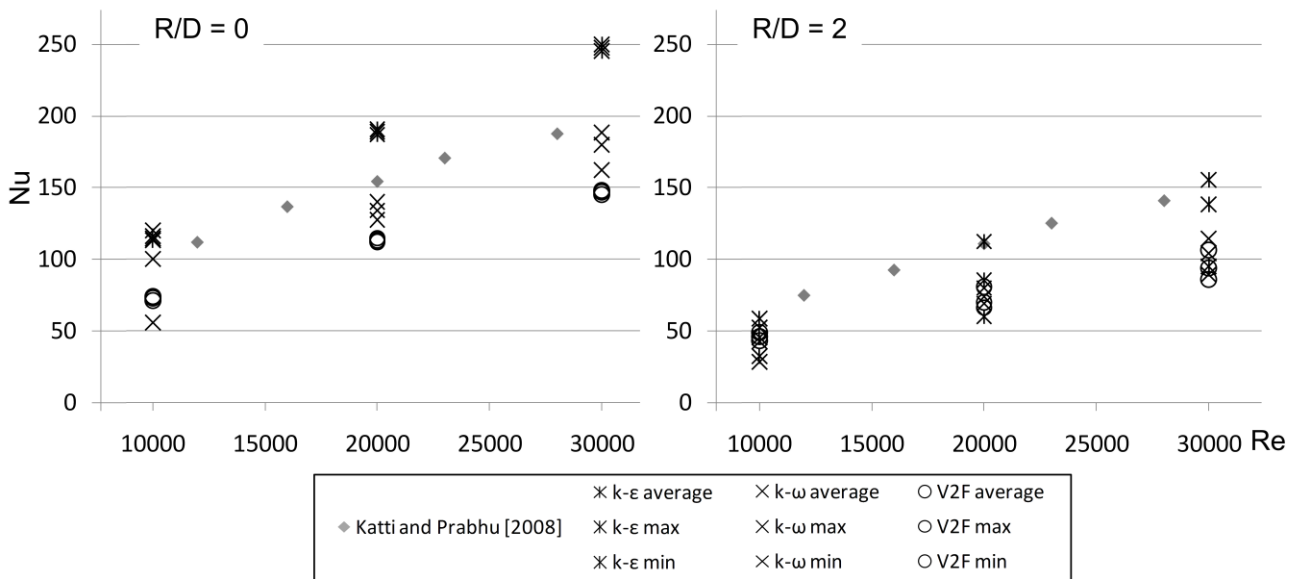


Figure 7. Effect of Re on the Nu at R/D=0 (stagnation point) and R/D = 2. Experimental data from Katti and Prabhu [2008]. For each turbulence model 3 values are presented: average, maximum and minimum. Note that their difference might be within graphical resolution (i.e. they overlap)

**Effect of Reynolds Number** For impinging jets the heat transfer is a strongly dependent on the Reynolds number. Figure 7 compares simulation results with experimental data for various Re at two different locations. Although the absolute values do not agree with the measured data, the main trend for Nu as function of Re at R/D = 0 is captured by all turbulence models. At higher R/D, results for the k-ε show a wide spreading deriving from its stronger dependency on other parameters. k-ω and V2F present a more consistent offset from the experimental data. These features support the results presented in Figure 5 which refer only to Re = 20000.

**Grid independency study** The selected group of cases used for the grid independency study is defined by the following parameters: Re =20000, k-ε and V2F, butterfly and peacock grid topology, grid density (0.25E06, 0.5E06, 1E06 and 2E06 cells). In general, no significant differences are found between the results obtained for grids with more than 0.5 E+06 cells. k-ε presents significant difference between results obtained with 0.25 E+06 and 0.5E+06 cells. V2F presents only minor differences between all the grids tested. This indicates that the degree of grid dependency varies with turbulence model.

**Effect of inlet velocity profile** The experimental data used for comparison in this work come from experiments performed with jets deriving from a fully developed pipe flow, while all simulations presented above are performed with uniform flow. Impinging jet heat transfer is a strong function of the Reynolds number as can be seen in Figure 7.  $Re$  is directly related to the flow momentum. A fully developed velocity profile has a higher flow momentum in the pipe centre compared to the corresponding uniform flow (i.e. for the same  $Re$ ). This affects the impinging jet heat transfer.

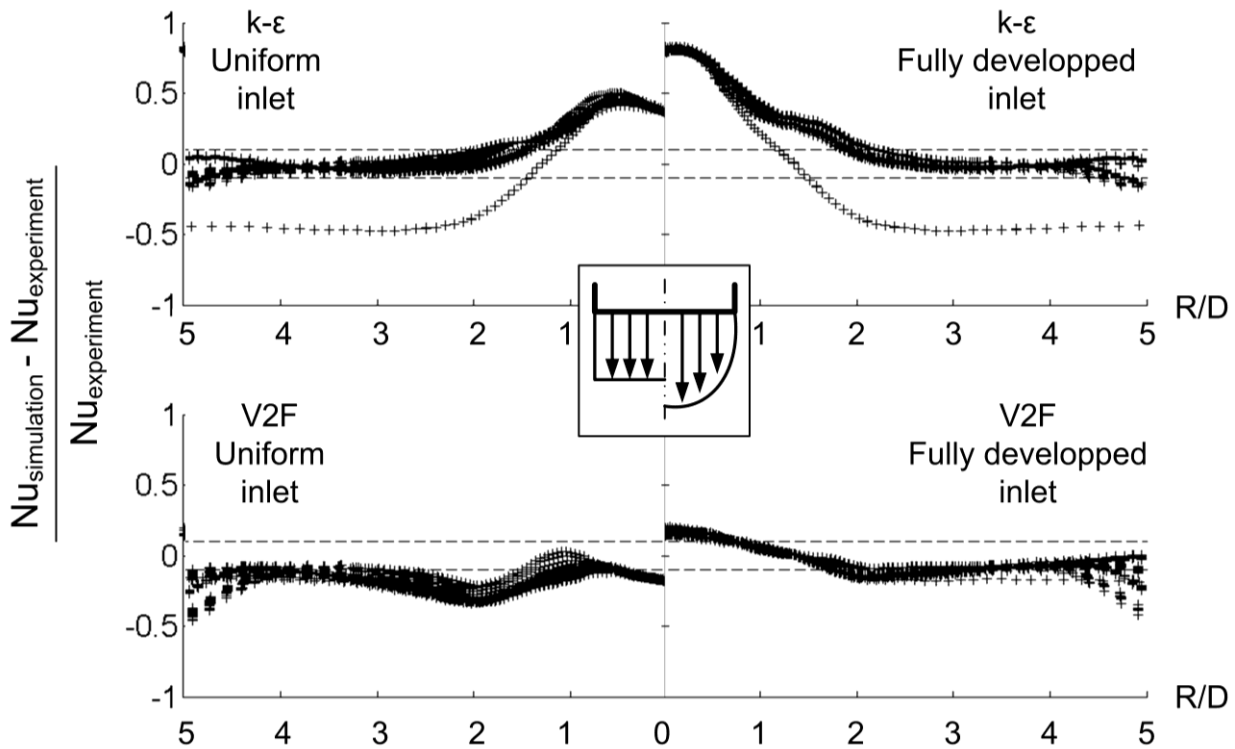


Figure 8. Effect of inlet velocity profile. Simulation results for  $Re = 20000$ , grid density  $0.5E+06$  and  $1E+06$ , butterfly and peacock grid topology. Comparison with linear interpolation of experimental results from Baughn and Shimizu [1989] and Katti and Prabhu [2008]. Available data from Baughn and Shimizu [1989] are scaled as in Figure 2. For each simulation all wall cell values are displayed. The  $\pm 0.1$  stripe represents 10% deviation from the experimental results interpolation according with statistical analysis

Simulations are run to study the effect of inlet velocity profile with the following parameters:  $Re = 20000$ ,  $k-\epsilon$  and V2F turbulence models, butterfly and peacock grid topology,  $0.5E+06$  and  $1E+06$  grid density. The applied velocity profile is obtained as described in the “modeling methodology” section. The velocity at the pipe center for the fully developed profile is about 1.23 times the velocity of a uniform flow profile (at  $Re = 20000$ ). Notably, the turbulent kinetic energy from the simulation is about twice the one used for the simulations with uniform flow inlet.

Results regarding the effect of the inlet velocity boundary profile are presented in Figure 8. The results obtained with V2F and fully developed inlet velocity profile agree with the experimental results almost within the estimated confidence of the experimental data.

For  $R/D < 2$  the effect of the velocity profile is very important as shown in Figure 8. For greater  $R/D$  the influence of the inlet conditions are negligible for  $k-\epsilon$  while some effects are still noticeable for the simulations performed with V2F.

**Flow field and heat transfer distribution** The comparison between simulation results and the experimental data showed good agreement for V2F. Results obtained with this model are used to get an insight of the flow field and its correlation to the heat transfer phenomena.

In Figure 9 the velocity field is compared for uniform and fully developed inlet flow. With the fully developed flow the jet has a considerably higher core velocity which is retained farther downstream the nozzle. Consequently, the jet is more compact and concentrates its effects on a smaller surface. As a result the heat transfer in the impingement zone is increased as can be seen in Figure 10.

The wall jet region is fed by the free stream jet. In the case with fully developed flow, the wall jet is fed within a smaller area, this can be clearly noticed through the difference in shape between the two cases in the inflection zone ( $R/D = 0.5$ ,  $H/D = 0.25$  in Figure 9). The result is a higher mass flow rate per unit cross section in the wall jet region, the flow is hence forced to a stronger acceleration, developing a higher velocity closer to the impingement point. The difference in the flow field is clear when analyzing the boundary layer velocity profile (bottom pictures in Figure 9). The flow field has a direct influence the heat transfer. The consequences of the flow field difference can be seen in Figure 10. The locations and the magnitude of the secondary peaks for  $Nu(R/D)$  are sensibly different for the two cases presented. The results obtained with the fully developed inlet velocity match the experimental results quite well, including the location and magnitude of the secondary peak.

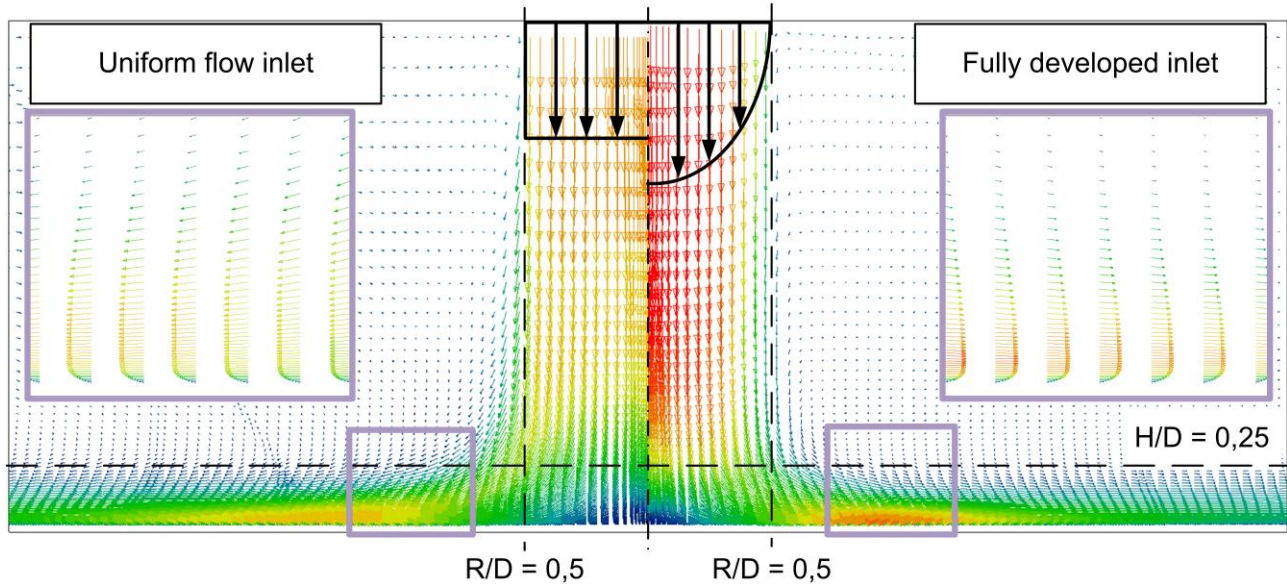


Figure 9. Comparison between uniform and fully developed inlet velocity profiles (qualitative illustration). Numerical simulation parameters ( $Re = 20000$ , V2F turbulence model,  $0.5E+06$  grid cells, peacock topology,  $2^{nd}$  order discretization scheme).

Data from all wall cells are plotted in Figure 10. The data scatter implies that the numerical solution is not perfectly axisymmetric. The data spreading is highest in the secondary peak area. Important transient phenomena are expected in this area where toroidal vortices created in the shear layer impact the target wall. Moreover, this study shows a relatively low convergence success (about 50%

considering all simulations performed). These results suggest that a representative axisymmetric steady state solution is difficult to achieve and a transient simulation approach might give considerably better results.

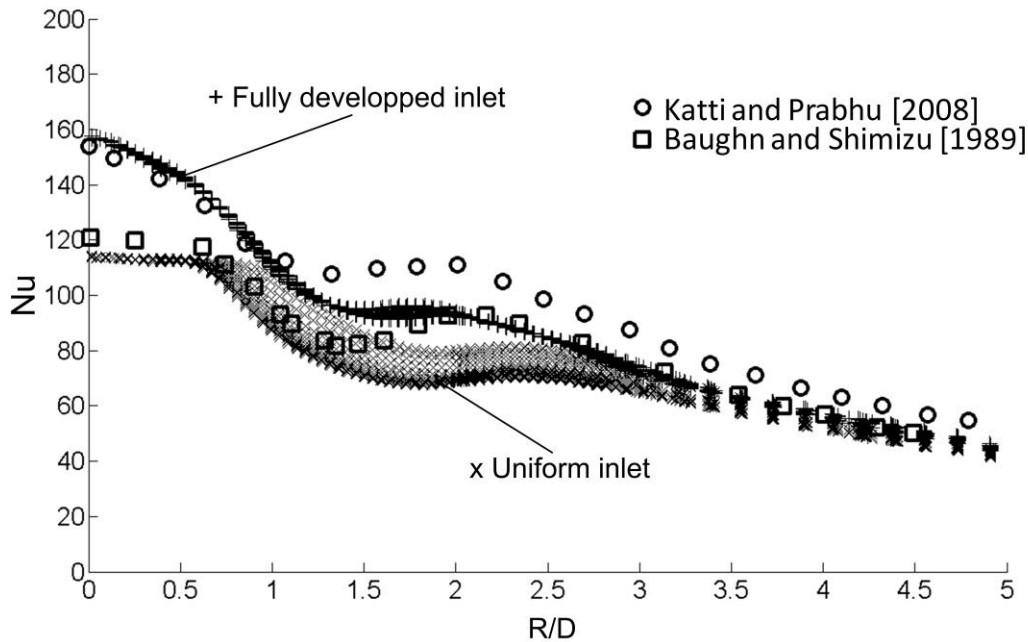


Figure 10. Nu(R/D) comparison between results with the V2F model and experiments at Re = 20000. Numerical simulation parameters (Re = 20000, V2F turbulence model, 0.5E+06 grid cells, peacock topology, 2<sup>nd</sup> order discretization scheme). Available data from Baughn and Shimizu [1989] are scaled as in Figure 2

## CONCLUSIONS

The present work can be seen as a best practice guide for steady CFD state modeling of impinging jets at H/D=2. As turbulence model V2F performs best. The peacock grid topology gives the best results both with respect to convergence robustness and accuracy in results. Finer grids give better results but show more often convergence problems. 2<sup>nd</sup> order numerical discretization gives slightly closer results to the experimental data than 1<sup>st</sup> order but encounters more often convergence problems. For all cases the choice of turbulence model has a much stronger influence on the results than the other variables (e.g. discretization order or grid density). Moreover, it is shown how grid independency is affected by the turbulence model. The inlet velocity profile has a significant influence on the simulation results. Uniform velocity profile cannot be used to represent fully developed velocity profile in these types of flows.

CFD simulation can be used to predict impinging jet heat transfer with accuracy close to experimental confidence. However, the task is not straight forward and careful model set up is necessary.

Two facts imply that important transient behavior prevent the simulation from reaching a converged steady state solution.

- The use of finer grid and higher numerical discretization order more often leads to non axisymmetric solutions but better agreement with the experimental data.
- The relatively low convergence success due to the cyclic oscillation of the residuals.

Significant transient phenomena are also measured by O'Donovan and Murray [2007] and pointed out as explanation for the peculiarity of impinging jet flows. It appears that impinging jets are very time-dependent and steady state simulations are inherently not capable of representing the physics correctly. If a higher precision is required a transient simulation approach should be considered instead of attempting steady state simulation with higher resolution (e.g. higher grid density).

## REFERENCES

- Baughn, J. W. and Shimizu S. [1989], Heat transfer measurements from a surface with uniform heat flux and an impinging jet, ASME J. Heat Transfer 111 1097.
- Durbin, P.A. [1995], Separated flow computations with the  $k-\epsilon-v^2$  model, AIAA Journal, 33(4), 659-664
- Gao, N., Sun H. and D. Ewing [2003], Heat transfer to impinging round jets with triangular tabs, Int. J. Heat Mass Transfer 46 2557–2569.
- Gao N. and Ewing D. [2006], Investigation of the effect of confinement on the heat transfer to round impinging jets exiting a long pipe, Int. J. of Heat and Fluid Flow 27 33–41.
- Lytle, D. and Webb B.W. [1994], Jet impingement heat transfer at low nozzle plate spacings, Int. J. Heat Mass Transfer 37 1687–1697.
- Lien, F.S., Chen, W.L. and Leschziner, M.A. [1996], Low-Reynolds-Number Eddy-Viscosity Modelling Based on Non-linear Stress-Strain/Vorticity Relations, Proc. 3<sup>rd</sup> Symp. on Engineering Turbulence Modelling and Measurements, Crete, Greece.
- Katti, V. and Prabhu S.V. [2008], Experimental study and theoretical analysis of local heat transfer distribution between smooth flat surface and impinging air jet from a circular straight pipe nozzle, Int. J. Heat Mass Transfer 51 4480–4495.
- O'Donovan T. S. and Murray D. B. [2007], Jet impingement heat transfer – Part I: Mean and root-mean-square heat transfer and velocity distributions, Int. J. Heat and Mass Transfer 50 3302–3314.
- Wilcox, D.C. [1998], Turbulence modelling for CFD, 2<sup>nd</sup> edition, DCW Industries, Inc.